

Supporting Information

Vacancy-coordinated Hydrogen Evolution Reaction for MoO_{3-x}

Anchored Atomically Dispersed MoRu Pairs

Suli Liu,^a Cheng Chen,^a Yuefeng Zhang,^b Qiuhui Zheng,^a Sudi Zhang,^a Xueqin Mu,^a Changyun Chen,^{*,a} Jianmin Ma^b and Shichun Mu^{*,c}

^aKey Laboratory of Advanced Functional Materials of Nanjing, Nanjing Xiaozhuang University, Nanjing 211171, China.

E-mail: cychen@njxzc.edu.cn

^bSchool of Physics and Electronics, Hunan University, Changsha 410082, China.

^cState Key Laboratory of Advanced Technology for Materials Synthesis and Processing, Wuhan University of Technology, Wuhan, Hubei 430056, China.

E-mail: msc@whut.edu.cn.

Experimental Details

Chemicals

The sodium molybdate dihydrate ($\text{Na}_2\text{MoO}_4 \cdot 2\text{H}_2\text{O}$), anhydrous ethanol, ammonia were all A. R. grade and purchased from Sinopharm Chemical Reagent Co. Ltd, China. poly-(diallyldimethylammonium chloride) (PDDA, 25 wt %) was purchased from Aladdin Aesar.

Synthesis of rGO-MoO_{3-x}-MoRu

Ambient temperatures, reduced graphene oxide (rGO, 60 mg) and deionized pure water (20 mL) were added to a three-necked flask reactor in sequence. After ultrasonication, a black solution was formed. Next, 3.5 mL PDDA was added and stirred for 5 h at 90 °C in an oil bath. After cooling to room temperature, washed with deionized water for several times, and then dried under vacuum at 60 °C, obtaining the PDDA-rGO nanosheets.

In a typical process, pre-synthesized PDDA-rGO (20 mg) were dispersed in double-distilled H₂O (100 mL) to form a homogeneous suspension. After ultrasonication, a black solution was formed. Then, $\text{Na}_2\text{MoO}_4 \cdot 2\text{H}_2\text{O}$ (0.0242 g, 0.1 mmol) aqueous solution (10 mL) was dropped into the above suspension under vigorous stirring. After 10 min, $[\text{Ru}(\text{NH}_3)_6]\text{Cl}_3$ solution (5 mL) that was obtained by dissolving $\text{RuCl}_3 \cdot x\text{H}_2\text{O}$ (0.0622 g, 0.3 mmol) in 25 wt % ammonia-water was rapidly added into the above mixture. By continuously stirring for 24 h, the composite precursors were obtained, which were separated and washed with deionized water and ethanol (volume ratio: 1:3) to remove byproducts. Those composite precursors were dried in vacuum and then placed in a horizontal furnace. After introducing high purity nitrogen, the furnace was heated to 700 °C at a rate of 2 °C min⁻¹ and kept at 700 °C for 1.5 h. Finally, it was naturally cooled down to room temperature. The black product was collected and used for analysis.

For comparison, rGO-MoO_{3-x}-MoRu with different oxygen vacancy contents were also prepared with the same procedure but in the different of temperature and Mo/Ru (different molar ratio), respectively.

Synthesis of rGO-Ru

rGO-Ru was prepared by a process similar to that of the typical sample (rGO-MoO_{3-x}-MoRu), except without using Na₂MoO₄·2H₂O.

Synthesis of rGO-MoO_{3-x}

rGO-MoO_{3-x} was prepared by a process similar to that of the typical sample (rGO-MoO_{3-x}-MoRu), except without using RuCl₃·xH₂O.

Characterization

The transmission electron microscopy (TEM) image was performed using a JEM-200CX instrument (Japan), and the corresponding acceleration voltage was 200 kV. Elemental mapping, scanning transmission electron microscopy (STEM) and EDS line-scan images was acquired using JEOL-2100F apparatus at an acceleration voltage of 200 kV. The powder X-ray diffraction (XRD) pattern was recorded using a D/max 2500VL/PC diffractometer (Japan) equipped with graphite monochromatized Cu K α radiation ($\lambda = 0.154060$ nm), and the corresponding scan range was 5° to 90° in 2 θ value. The X-ray photoelectron spectra (XPS) were recorded on a scanning X-ray microprobe (PHI 5000 Versa, ULACPHI, Inc.) that uses Al K α radiation. The binding energy of the C1s peak (284.6 eV) was employed as a standard to calibrate the binding energies of other elements.

The XANES and EXAFS measurement

The X-ray absorption near-edge structure (XANES) and extended X-ray absorption fine structure (EXAFS) of the Mo and Ru K-edges were conducted on the XAFS station of the 14W1 beam line of the Shanghai Synchrotron Radiation Facility, which operated at approximately 300 mA and 3.5 GeV. The reference Mo-foil, MoO₃-foil and Ru-foil, with purities of 99.99%, were purchased from the Kunming Institute of Precious Metals of China. All the samples were measured as fine powders (<200 mesh) which were coated onto Scotch Magic Tape (3M 811) without using any dilution materials. The X-ray absorption spectra of Mo and Ru K-edge of all the samples were recorded in fluorescence mode. A Si (311) double-crystal monochromator was used to monochromatize the X-ray radiation, and a partial detuning between the silicon crystals was performed to suppress the large amount of harmonics. The back-subtracted EXAFS function was converted into k space and weighted by k² to compensate for the

diminishing amplitude due to the decay of the photoelectron wave. The Fourier transforming of the k^2 -weighted (for Mo) and k^3 -weighted (for Ru) EXAFS data was performed in the range of $k = 3.5$ - 14 \AA^{-1} using a Hanning function window to obtain the radial distribution function (RDF).

Electrochemical Tests

Electrochemical HER measurements. The electrochemical HER experiments were carried out using a CHI 660E electrochemical workstation (Shanghai, Chenhua Co.) with a standard three electrode system. A graphite rod and Ag/AgCl (3 M KCl) served as the counter electrode and reference electrode, respectively. All the potentials were referenced to a reversible hydrogen electrode (RHE). A glassy carbon electrode (3 mm in diameter) was used in the HER experiments. All the electrochemical measurements were carried out in N_2 -versus O_2 -saturated atmosphere at room temperature. In 0.5 M H_2SO_4 , the CV tests were conducted using a potential window of -0.8 V to 0.2 V (vs. Ag/AgCl) and polarization curves were obtained using a potential window of -0.8 V to 0 V (vs. Ag/AgCl) after iR compensation with a scan rate of 5 mV s^{-1} . All the potentials were referenced to a reversible hydrogen electrode (RHE) by adding a value of 0.21. In 1.0 M KOH, the CV tests were conducted using a potential window of -1.5 V to -0.5 V (vs. Ag/AgCl) and polarization curves were obtained using a potential window of -0.5 V to -1.4 V (vs. Ag/AgCl) after iR compensation with a scan rate of 5 mV s^{-1} . All the potentials were referenced to a reversible hydrogen electrode (RHE) by adding a value of 1.02.

Theoretical Methods

All the geometric optimizations, single-point energies and electronic structures calculations are performed through the spin-polarized density functional theory method by using the Cambridge Serial Total Energy Package (CASTEP) code on the basis of the plane-wave pseudopotential. The Perdew–Burke–Ernzerhof (PBE) exchange-correlation functional for generalized gradient approximation (GGA) and the projector augmented wave (PAW) method explaining the core-valence interactions are employed. The cutoff energy for plane-wave basis is set to 400 eV, and the reciprocal space is sampled by Γ -centered Monkhorst-Pack scheme with a grid of $3 \times 3 \times 1$. The

electronic relaxation is performed to within an energy tolerance of 10^{-5} eV for self-consistency, while ionic optimizations are performed until all the residual forces are smaller than 0.01 eV/Å. Spin-polarized wave functions are used for all calculations. Other than these, we have set a vacuum region of 15 Å along the z-direction to avoid interactions between adjacent images. For adsorption studies, a $4 \times 2 \times 1$ and $3 \times 2 \times 1$ supercell is built for Ru (100) surface and MoO₃ (040) surface, respectively. The complexation between Ru (100) surface and MoO₃ (040) surface is theoretically achieved by constructing a heterojunction comprising 80 atoms.

The adsorption energies of intermediates on the catalyst surfaces is defined as follows:

$$E_{ad} = E_{adsorbate/surface} - E_{adsorbate} - E_{surface}$$

Where $E_{adsorbate/surface}$, $E_{adsorbate}$ and $E_{surface}$ are the total energy of the adsorption system, adsorbate in vacuum and the clean surface, respectively. By this definition, if the value of E_{ad} is negative, it implies that this process is an exothermic process. In general, the more negative this value is, the more stable it is.

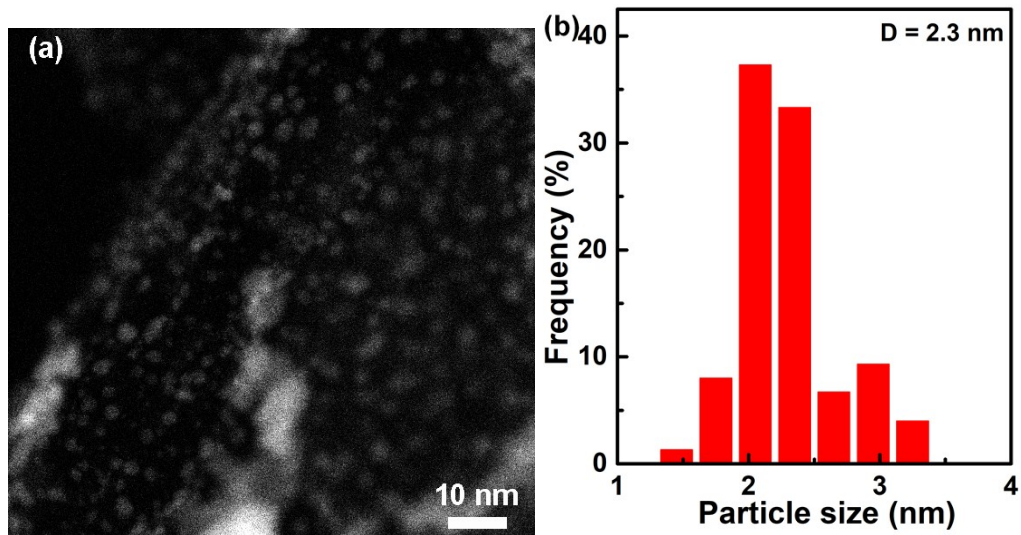


Fig. S1 (a) Atomic-resolution HAADF-STEM and (b) Diameter distribution image of surface-decorated nanoparticles in rGO-MoO_{3-x}-MoRu.

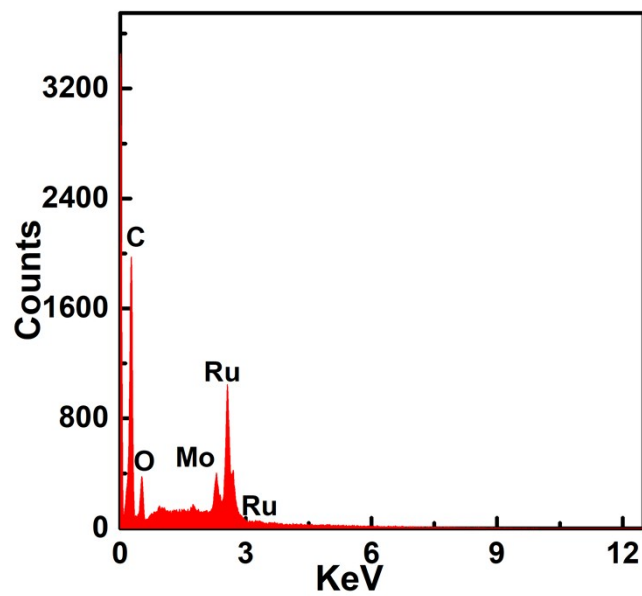


Fig. S2 EDS image of rGO-MoO_{3-x}-MoRu.

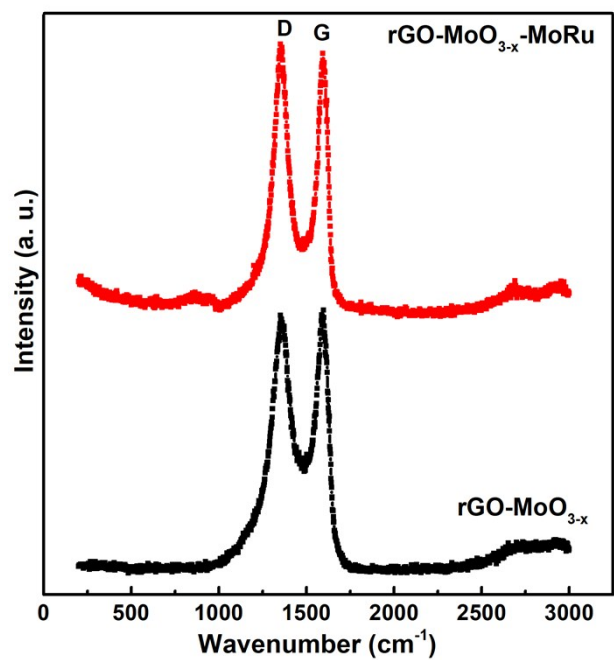


Fig. S3 Raman spectrum analyses of $rGO-MoO_{3-x}$ and $rGO-MoO_{3-x}-MoRu$ samples.

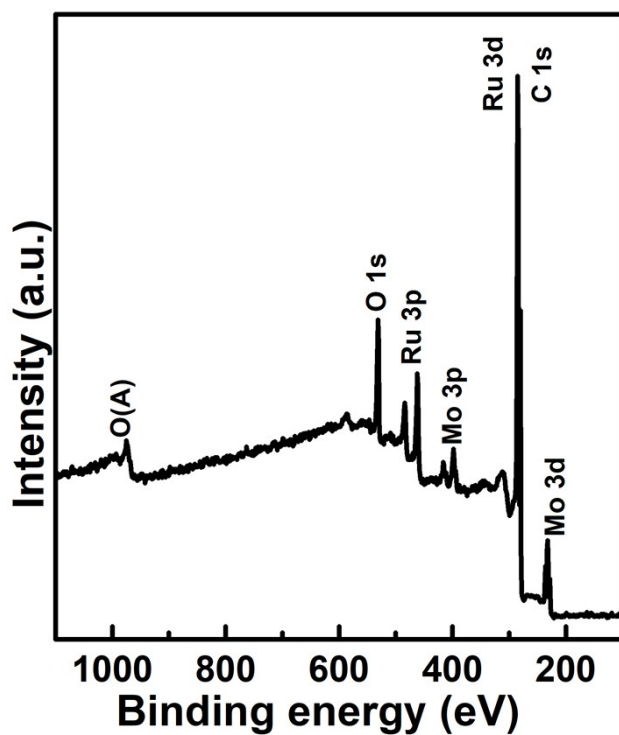


Fig. S4 XPS survey scan spectra of $rGO-MoO_{3-x}-MoRu$ samples.

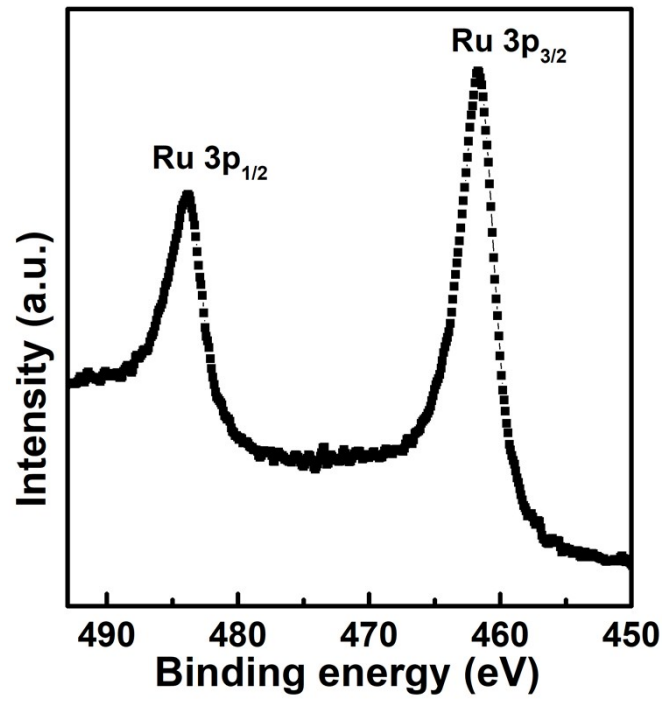


Fig. S5 XPS spectra of Ru 3p of rGO-MoO_{3-x}-MoRu NCs.

Table S1. EXAFS fitting parameters at the Mo and Ru K-edge for various samples ($S_0^2=0.952$ (Mo), 0.740 (Ru))

Sample	Shell	N^a	$R(\text{\AA})^b$	$\sigma^2(\text{\AA}^2)^c$	$\Delta E_0(\text{eV})^d$	R factor
Mo foil	Mo-Mo	8	2.73	0.0040	-5.8	0.0021
	Mo-Mo	6	3.14	0.0040		
rGo-MoO ₃	Mo-O	3.6	2.03	0.0281	-2.0	0.0386
	Mo-Mo	4.7	3.13	0.0165		
rGo-Ru-MoO ₃	Mo-O	2.1	2.08	0.0251	0.3	0.0164
	Mo-Mo	6.0	2.81	0.0277		
Ru foil	Ru-Ru	12	2.67	0.0034	1.7	0.0039
rGo-Ru-MoO ₃	Ru-Mo	10.5	2.72	0.0049	-6.1	0.0120

^a N : coordination numbers; ^b R : bond distance; ^c σ^2 : Debye-Waller factors; ^d ΔE_0 : the inner potential correction. R factor: goodness of fit. S_0^2 was set to 0.952 (Mo) and 0.740 (Ru), according to the experimental EXAFS fit of Mo and Ru foil by fixing CN as the known crystallographic values.

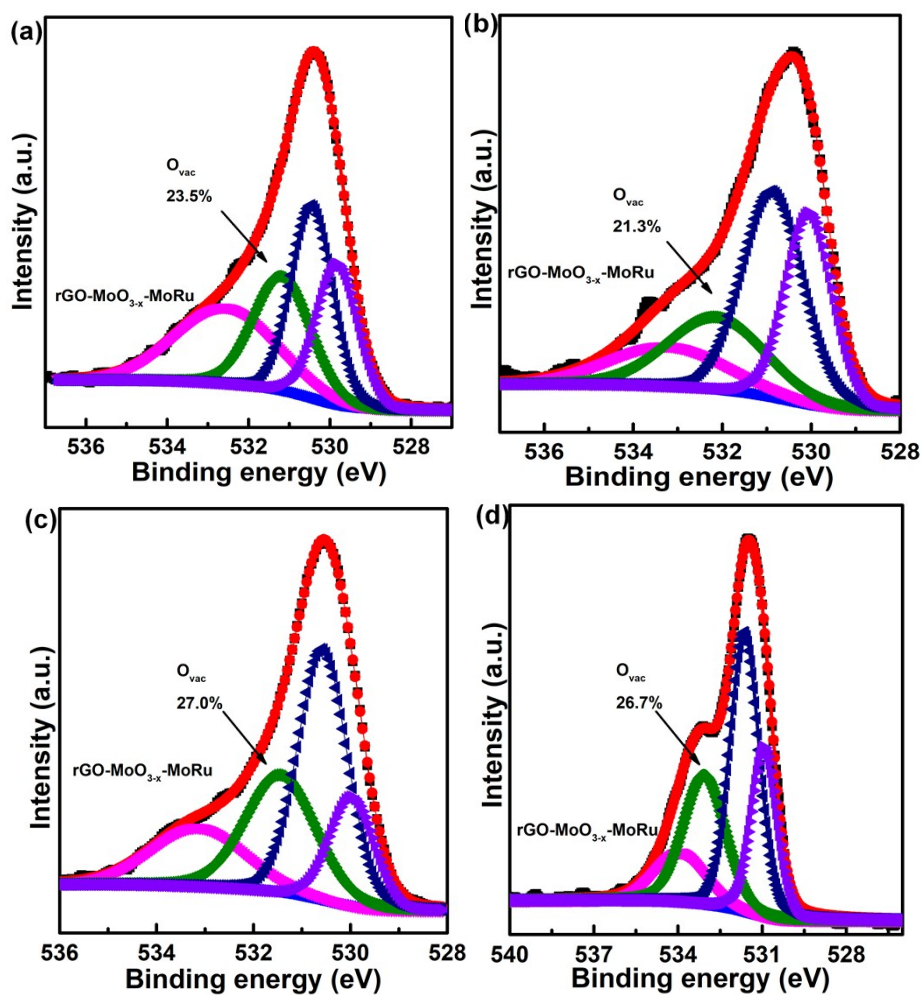


Fig. S6 Fitted O1s spectra for (a) rGO-MoO_{3-x}-MoRu (Mo:Ru = 1:1); (b) rGO-MoO_{3-x}-MoRu (Mo:Ru = 1:5); (c) rGO-MoO_{3-x}-MoRu (500 °C), and (d) rGO-MoO_{3-x}-MoRu (900 °C), respectively.

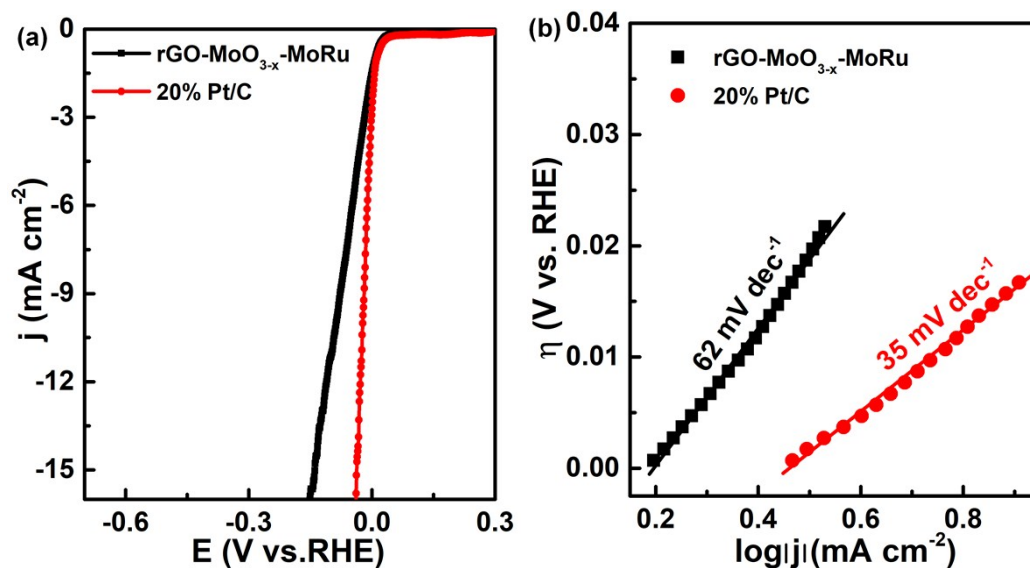


Fig. S7 (a) LSV curves and (b) Tafel plots using rGO-MoO_{3-x}-MoRu NCs and 20% Pt/C in 1 M PBS solution at a scan rate of 5 mV s⁻¹.

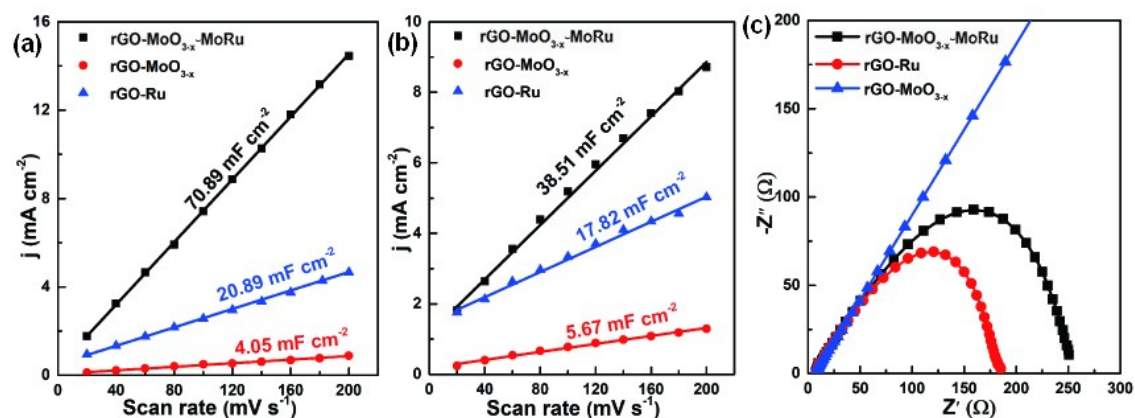


Fig. S8 (a, b) The capacitive current densities as a function of the scan rate for rGO-MoO_{3-x}-MoRu, rGO-MoO_{3-x} and rGO-Ru in 0.5 M H₂SO₄ and 1.0 M KOH. (c) Nyquist plots of various catalysts.

Table S2. Comparison of the electrocatalytic HER properties of some recently reported catalysts in 1.0 M KOH

Catalysts	Tafel slope [mV dec ⁻¹]	η_{10} [mV]	Ref.
rGO-MoO _{3-x} -MoRu	25	20	This work
Ni@Ni ₂ P-Ru HNRs	41	31	<i>J. Am. Chem. Soc.</i> , 2018 , <i>140</i> , 2731.
RuCo@NC	31	28	<i>Nat. Commun.</i> , 2017 , <i>8</i> , 14969.
NiCo ₂ P _x	34.3	58	<i>Adv. Mater.</i> , 2017 , <i>29</i> , 1605502.
Ni _{0.89} Co _{0.11} Se ₂ MNSN/NF	52	85	<i>Adv. Mater.</i> , 2017 , <i>29</i> , 1606521.
Ni-P/carbon paper	85.4	100	<i>Adv. Funct. Mater.</i> , 2016 , <i>26</i> , 4067.
Ni-NiO/N-rGO	46	135	<i>Adv. Funct. Mater.</i> , 2015 , <i>25</i> , 5799.
CoP@NC	58	129	<i>ACS Catal.</i> , 2017 , <i>7</i> , 3824-3831.
S-MoP NPL	56	104	<i>ACS Catal.</i> , 2019 , <i>9</i> , 651-659.
meso FeS ₂	78	96	<i>J. Am. Chem. Soc.</i> , 2017 , <i>139</i> , 13604-13607.
PtNi-O/C	78.8	39.8	<i>J. Am. Chem. Soc.</i> , 2018 , <i>140</i> , 9046-9050.
Co-P/RGO	38	150	<i>Chem. Sci.</i> , 2016 , <i>7</i> , 1690-1695.
Ni ₉ S ₈	123.3	230	<i>Adv. Funct. Mater.</i> , 2016 , <i>26</i> , 3314-3323.
NiCo ₂ S ₄	58.9	210	<i>Adv. Funct. Mater.</i> , 2016 , <i>26</i> , 4661-4672.
NiFe LDH	42	158	<i>Adv. Energy Mater.</i> , 2016 , <i>6</i> , 1502585.
Co-P	63	180	<i>J. Mater. Chem. A</i> 2016 , <i>4</i> , 7549-7554.
Ni@C-400	95	110	<i>J. Mater. Chem. A</i> , 2016 , <i>4</i> , 7297-7304.
NiSe/NF	120	96	<i>Angew. Chem. Int. Ed.</i> , 2015 , <i>127</i> , 9483-9487.
NiO/Ni-CNT	51	100	<i>Nat. Commun.</i> , 2014 , <i>5</i> , 4695.
B-Mo ₂ C	55	112	<i>Angew. Chem. Int. Ed.</i> , 2015 , <i>54</i> , 15395-15399.
Ni ₅ P ₄	53	150	<i>Angew. Chem. Int. Ed.</i> , 2015 , <i>127</i> , 12538-12542.
MoS ₂ /Ni ₃ S ₂	83	110	<i>Angew. Chem. Int. Ed.</i> , 2016 , <i>128</i> , 6814-6819.
Mo ₂ C/NCF	65	100	<i>ACS Nano</i> , 2016 , <i>10</i> , 11337-11343

Table S3. Comparisons of electrocatalytic HER properties of some recently reported catalysts in 0.5 M H₂SO₄.

Catalyst	Tafel slope [mV dec ⁻¹]	η_{10} [mV] ^[1]	Ref.
rGO-MoO _{3-x} -MoRu	40	60	This work
NiCo ₂ P _x	59.6	104	<i>Adv. Mater.</i> , 2017 , <i>29</i> , 1605502.
MoS ₂ /CoSe ₂	36	68	<i>Nat. Commun.</i> , 2015 , <i>6</i> , 5982.
MoP	45	90	<i>Chem. Mater.</i> , 2014 , <i>26</i> , 4826.
CoP/CNT	54	122	<i>Angew. Chem. Int. Ed.</i> , 2014 , <i>53</i> , 6710.
WS ₂ /WO ₂ -6 NRs	63	147	<i>ACS Catal.</i> , 2016 , <i>6</i> , 6585-6590.
MoS ₂ /MoO ₂ -6 NRs	51	190	<i>ACS Catal.</i> , 2016 , <i>6</i> , 6585-6590.
CoP@NC	49	78	<i>ACS Catal.</i> , 2017 , <i>7</i> , 3824-3831.
NPNi-MoS ₂ /RGO	71.3	205	<i>ACS Catal.</i> , 2018 , <i>8</i> , 8107-8114.
MoS ₂ HG	41	124	<i>ACS Catal.</i> , 2018 , <i>8</i> , 1828-1836.
CoS ₂ NW	51.6	145	<i>J. Am. Chem. Soc.</i> , 2014 , <i>136</i> , 10053-10061.
CoS ₂ /P	50	67	<i>Chem. Commun.</i> , 2015 , <i>51</i> , 14160-14163.
MoP	60	246	<i>Chem. Commun.</i> , 2014 , <i>50</i> , 11683-11685
1T' ReSe ₂	50.8	123	<i>J. Am. Chem. Soc.</i> , 2018 , <i>140</i> , 8563-8568.
1T' ReSSe	50.1	84	<i>J. Am. Chem. Soc.</i> , 2018 , <i>140</i> , 8563-8568.
W@NPC	191	233	<i>J. Am. Chem. Soc.</i> , 2017 , <i>139</i> , 5285-5288.
MoP ₂	63.6	58	<i>J. Mater. Chem. A</i> , 2016 , <i>4</i> , 7169-7173.
MoP	50	150	<i>J. Mater. Chem. A</i> , 2015 , <i>3</i> , 4368-4373.
MoS ₂ nanosheet	43	187	<i>J. Am. Chem. Soc.</i> , 2013 , <i>135</i> , 10274-10277.
MoS ₂ nanoparticles	62	118	<i>ACS Nano</i> , 2014 , <i>8</i> , 4940-4947.
CoP/CC	51	67	<i>J. Am. Chem. Soc.</i> , 2014 , <i>136</i> , 21,7587-7590
NiP ₂ NS/CC	51	75	<i>Nanoscale</i> , 2014 , <i>6</i> , 13440-13445.
Au-MoS ₂	71	263	<i>J. Am. Chem. Soc.</i> , 2015 , <i>137</i> , 7365-

			7370.
Porous MoO ₂ /MoS ₂	76.1	242	<i>Nanoscale</i> , 2015 , 7, 5203-5208.
Zn-MoS ₂	51	140	<i>J. Am. Chem. Soc.</i> , 2017 , 139, 43, 15479-15485.
MoS ₂ /3D-NPC	51	220	<i>Nanoscale</i> , 2015 , 7, 18004-18009.
MoS _x -NCNT	40	110	<i>Nano Lett.</i> , 2014 , 14, 1228-1233.
1T MoS ₂	43	153	<i>J. Am. Chem. Soc.</i> , 2016 , 138, 7965-7972.

[1] The potential measured versus RHE.

[2] j_0 values were calculated from tafel curves using an extrapolation method.